Energy scattering of hybrid FE-SEA model with nonlinear joints

Puxue Tan[a], Sebastiano Fichera[a], Anas Batou[a,*]

[a] *University of Liverpool, School of Engineering, Brownlow Hill, Liverpool, L69 3GH, UK*

Abstract

Nonlinearity in structures causes energy scattering between different frequency ranges. This paper proposes a new hybrid FE-SEA formulation to analyse complex structures with nonlinear deterministic components. The formulation is derived in two stages. First the governing equation for deterministic components in time domain is transformed to frequency domain using the method of harmonic balance and the Galerkin method. Equivalent stiffness method is then applied in frequency domain to linearise the nonlinear terms. The second process is regarded to the derivation of the hybrid model. Based on a proposed nonlinear energy transfer model and the linearisation in the first stage, the linearised hybrid FE-SEA governing equation is derived, and the iterative procedure is given. For validation purpose, nonlinear Lagrange-Rayleigh-Ritz method plus Monte Carlo simulation is used as the benchmark model. Two case studies are applied for validation and investigation of the coupling loss factor (CLF). The coupling between subsystems at different frequencies can be reflected by the CLF. Good agreements between the benchmark model and proposed hybrid model can be observed.

Keywords: hybrid FE-SEA, localised nonlinearity, energy scattering, equivalent linearisation

1. Introduction

Noise and vibration predictions for complex structural systems are computationally challenging due to the existence of uncertainties and the very large number of degrees of freedom (DoFs). In the structural dynamic analysis of engineering systems, e.g. aircraft, ships, the use of deterministic models is not efficient and reliable enough to calculate the response in mid- and high- frequency range. Hence, specific methods for structural modelling with the presence of uncertainties are required. The statistical energy analysis (SEA) was presented by Lyon to obtain very efficiently system-level responses for statistical components (subsystems) of the complex structures in high-frequency range [1, 2]. This method assumes that the uncertainties yield absolute overlaps between the high-frequency structural modes enabling the assumption of equivalence between the frequency-band-averaged energy and the ensemble average energy [3, 4]. The SEA model assumes that the energy flowing into the subsystem equals the sum of energy dissipated and transmitted to other subsystems. The energy transmitted to other subsystems is proportional to the energy difference between the subsystems through a parameter called the coupling loss factor (CLF) [5, 6].

Compared to the high-frequency response prediction, mid-frequency problems are different because the uncertainty has different effects on the structural modes. Responses of some stiffer structural components

*Corresponding author
Email address: batoua@liverpool.ac.uk (Anas Batou)

in mid-frequency range are robust to uncertainties, and the deterministic methods, e.g. finite element (FE) method, are more suitable for these components. But some other more flexible components are vulnerable to uncertainties, and the SEA is more suitable to model these components. A powerful method, the hybrid FE-SEA, was proposed to solve the mid-frequency problem for noise and vibration in complex structures [7, 8]. The subsystem is modelled by the wave approach in which the motions in direct fields and reverberant fields meet the reciprocity relation [9]. Moreover, under the framework of the hybrid FE-SEA model, other hybrid formulations, e.g. Wave Based-SEA, Boundary Element-SEA etc., were proposed to save computational time or solve the problems under particular conditions [10, 11, 11, 12, 13]. In addition to the ensemble average energy, the variance of the energy was also discussed for both SEA and hybrid FE-SEA models [4, 14, 15, 16, 17].

The SEA and its hybrid models mentioned above are based on linear assumption. But in fact, nonlinearities may be non-negligible in engineering structures and then the use of linear methods would not be suitable and accurate. In structural vibration, the nonlinearity leads to internal resonances, sub-resonances and other types of resonant phenomena, and even other more complex dynamics, e.g. bifurcation. Hence, considering the hybrid FE-SEA under nonlinear situations is necessary for engineering application. One approach taking account the nonlinearity within SEA framework is the entropy-based SEA model [18, 19, 20]. This model is an analogy of thermodynamics but still limited to high-frequency range. Another approach is to apply the equivalent stiffness method to the hybrid model where the nonlinearity is localised in deterministic components [21, 22, 23]. These approaches essentially linearise the nonlinear stiffness in time domain, and then apply the equivalent stiffness to frequency domain. Hence, this frequency-domain responses do not include the frequency coupling effects, because the stiffness strengthening and reduction has been averaged into all frequency range. However, there exists another important nonlinear phenomenon: energy scattering (or energy cascade) [24]. Nonlinearity leads the responses at different frequencies to interact over each other, or some of the modes are coupled because of nonlinearity. Even at the frequency point where the external force amplitude is zero, the energy response can also be very significant due to the energy scattering. In the reference [24] the authors investigated the energy scattering of hybrid FE-SEA, and the proposed method, under many linearisation assumptions, enabled the construction of the trends of the response [24].

This paper proposes a new hybrid FE-SEA model taking consideration of localised nonlinearity in the FE components. Different from the previous formulations, equivalent stiffness method is applied in frequency domain but not in the time domain, and the energy scattering under different frequencies is considered. In order to realize the nonlinear governing equation in frequency domain, the method of harmonic balance (MHB) combined with Galerkin method are used for the transformation from time domain to frequency domain. Then a set of nonlinear algebraic equations (frequency domain) can be obtained. This algebraic equation can be linearised by a technique analogous to statistical linearisation (SL) [25], by which the relation between equivalent stiffness and the nonlinear stiffness can be established. This relation represented by a linear equation can be used to update the equivalent stiffness in iterative steps. The new nonlinear FE-SEA formulation is then given in this paper. It should be noted that this paper derives the formulation referred to the nonlinear deterministic components with multi-DoFs (MDoFs). This paper only focuses on cubic nonlinearity in the derivation process, but the formulation provides a general framework that can include

other form of nonlinearities, e.g. quadratic nonlinearity.

The second section in this paper describes the new energy transfer model for the nonlinear system with uncertainties, and also introduces some assumptions. The third section is devoted to derive the equivalent stiffness equation and the governing equation for the nonlinear model. The forth section derives the governing equation of the benchmark model of the spring-mass-plate structure, and based on this model, the fifth section gives two case studies for validation.

2. Hybrid FE-SEA model and assumptions

This section gives the overview of FE-SEA model proposed by Shorter and Langley [7]. Basic principles and key steps in the FE-SEA framework which are used in later derivation are introduced. Moreover, some assumptions related to nonlinear FE-SEA model are introduced to support the derivation.

The principles used to establish the governing equation of hybrid FE-SEA model are the same as the traditional SEA method, which are the energy conservation and the property that the energy input into a subsystem equals the sum of the energy dissipated and the energy transferred to other subsystems. The difference is that the deterministic components introduce the deterministic boundaries of the subsystems, which requires different coupling relations. In the hybrid FE-SEA model, the viewpoint of the wave approach is adopted to describe the statistical fields (subsystems) which is the superposition of direct fields and reverberant fields. The power transmission follows the energy conservation, which can be depicted in Fig. 1. It can be observed that the power input into the subsystem is transmitted to direct fields first, the reflection of the wave due to random boundaries transmits the power from direct fields to reverberant fields. Then some of the power is dissipated and the other is an output to other components including both deterministic and indeterministic components. The key to construct the governing equation is to obtain the relation between direct fields and reverberant fields, and this has also been achieved by Shorter and Langley. [9].

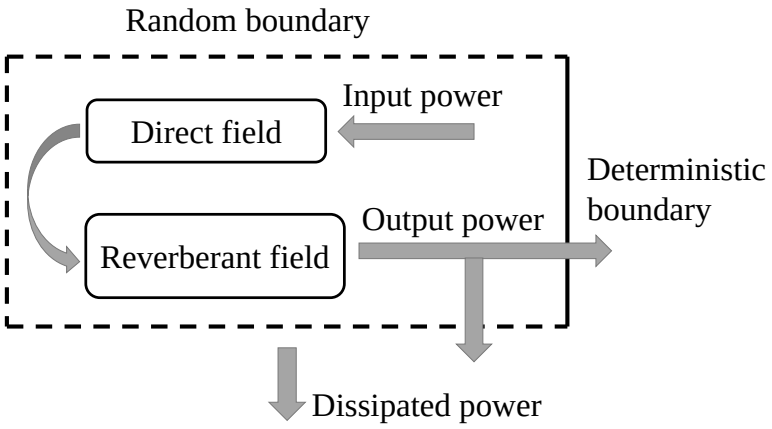

Figure 1: Power transmission within a subsystem.

In the cases of linear deterministic components (joints), responses (ensemble average energy) under different frequencies are not coupled, and the energy scattering is not considered. The energy transfer between the statistical fields in this situation only happens at the same frequency, as shown in Fig.2. Moreover, this

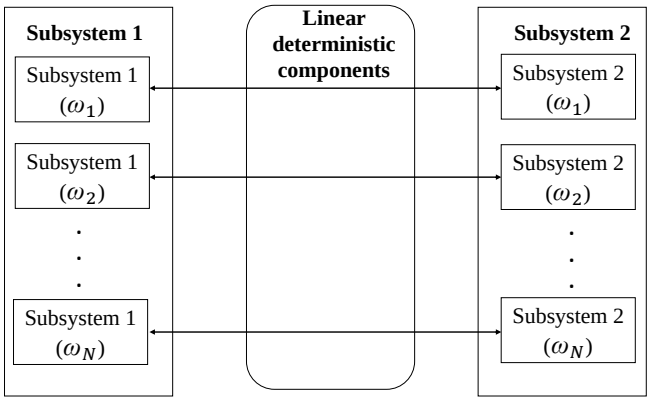

Figure 2: Energy transfer between subsystems for linear systems.

leads to the convenience that the response can be obtained at selected frequency points separately. However, for complex structures with nonlinear deterministic joints, the nonlinearity causes internal resonances, sub-resonances and other types of nonlinear resonance phenomena. These resonances yield interactions between input and response in different frequency points. Hence, it is not proper to calculate the response at certain frequencies separately. For the hybrid FE-SEA model, the energy scatters between different frequency ranges. The energy transfer, both between modes in different frequencies and within or between subsystems, should be considered. Hence, this paper proposes an energy transfer model for subsystems at different frequencies as shown in Fig.3. It shows that, under the effects of nonlinear deterministic joints, subsystem 1 at a dis-

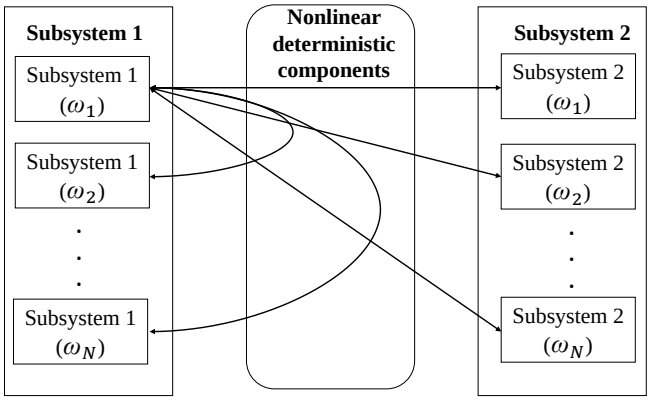

Figure 3: Energy transfer between or within subsystems for nonlinear system.

cretized frequency point 1ω is coupled with subsystem 1 from 2ω to $N\omega$ and subsystem 2 from 2ω to $N\omega$. This coupling happens only because of the nonlinearity. Even within the subsystem, the statistical fields themselves at different frequencies are linear and uncoupled to each other, but interactions occur due to the presence of nonlinear joints. For terminology convenience, we treat the subsystem at a certain frequency as a stand-alone subsystem. For instance, if the original linear model has N_s subsystems and the number of

selected discrete frequency points is N_ω, the total number of subsystems for the nonlinear model is $N_s \times N_\omega$.

The classic hybrid FE-SEA model is linear and built in frequency domain. Hence, the first step to solve build the nonlinear FE-SEA governing equation is to obtain the frequency-domain governing equation for nonlinear deterministic components. Linearisation procedure is used. The combination of MHB and Galerkin method has shown its effectiveness in this process [26]. We apply this method in this paper. The next step is to obtain the linearisation relation between the equivalent stiffness and nonlinear terms. Since the responses of nonlinear components are ensemble random, a linearisation technique is used in this paper. This technique is analogous to the SL [25], but the difference is that the SL is applied to time-domain governing equation, and the technique in this paper is based on frequency domain. It should be noted that the SL is related to random vibration in which the inputs are stochastic, and the response in time domain is random. But in this paper, for just one ensemble of the structure, the response is random only if the input is assumed as rain-on-the-roof, while it is not random if the input is harmonic. However, for a large number of ensembles, the displacement responses in frequency domain can still be described as statistical. And the weak nonlinearity assumption enable to assume that the probability distribution is close to those in linear cases. For linear structural ensembles, displacement responses do not follow exact Gaussian distribution with harmonic inputs. But massive explorations have been made to structural ensembles to show that the distribution can be Gaussian-level. And, in this paper, the displacement responses of structural ensembles are assumed to satisfy some Gaussian properties. This assumption is fundamental to the linearisation process in the derivation.

Even though the MHB can be used regardless of weak or strong nonlinearity, the equivalent stiffness method in this paper is based on weak nonlinearity hypothesis. This paper assumes the nonlinear response can be approximated by linear iteration. The weak nonlinearity assumption allows to assume that the equilibrium points of the nonlinear joints are very close to the one for linear models which is zero.

3. Nonlinear deterministic modelling and the hybrid model

This section is devoted to the derivation of the governing equation for the hybrid model with nonlinear deterministic components. The first step is to derive the equation for equivalent stiffness from the nonlinear governing equation of deterministic component by deterministic modelling. Then the second step is to obtain the hybrid model by using equivalent stiffness based on the energy transfer model in Fig.3.

3.1. Method of harmonic balance and equivalent linearisation

Nonlinear modelling for deterministic component with N_d degrees of freedoms (DoFs) can be applied and gives following nonlinear governing equation in time domain

$$m_j \ddot{u}_j + c_j \dot{u}_j + k_j^{(a)} u_j + \sum_{smn}^{N_d} k_{jsmn}^{(b)} u_s u_m u_n = f_j^{ex} \ , \tag{1}$$

where m_j and c_j are j-th generalized mass and damping for the structural system; u_j is j-th generalized displacement; $k_j^{(a)}$ is the generalized linear stiffness; $k_{jsmn}^{(b)}$ is the coefficient for cubic nonlinearities. The harmonic motion and input for deterministic component is assumed and hence the response and external

force can be written as the following series form

$$u_j = \sum_{\substack{l=-N_\omega \\ l\neq 0}}^{N_\omega} \overline{u}_{jl}\, e^{i\, l\omega t} \ , \tag{2}$$

$$f_j^{ex} = \sum_{\substack{l=-N_\omega \\ l\neq 0}}^{N_\omega} \overline{f}_{jl}^{ex}\, e^{i\, l\omega t} \ , \tag{3}$$

where ω is the frequency spacing between selected frequency points; i denotes the imaginary unit; $\overline{u}_{jl}$ is the l-th coefficient for u_j at the discretized frequency $l\omega$; N_ω is the number of single-side frequency points. It is noted that these two equations introduce the responses containing both positive and negative (double-side) frequencies. It has to be ensured that the responses of a pair are conjugate and fully correlated. For instance, if two frequencies are opposite numbers, e.g. $l\omega = -p\omega$, then the amplitudes related to these two frequencies are conjugate and share the same statistics for both real and imaginary parts. In order to make the formulas simple and clear, the lower limit of the symbol $\sum_{\substack{l=-N_\omega \\ l\neq 0}}^{N_\omega}$ is omitted and it is simplified to $\sum_l^{N_\omega}$ in the following derivation.

Substituting Eqs.(2) and (3) into Eq.(1), and applying the MHB yield the following residual

$$\epsilon_j^{H1} = \sum_l^{N_\omega} \overline{u}_{jl}\, e^{i\, l\omega t}(-l^2\omega^2 m_j + il\omega c_j + k_j^a) + \sum_{smn=1}^{N_d} k_{jsmn}^b \sum_{lpq}^{N_\omega} \overline{u}_{sl}\overline{u}_{mp}\overline{u}_{nq}\, e^{i\,(l+p+q)\omega t} - \sum_l^{N_\omega} \overline{f}_{jl}^{ex}\, e^{i\, l\omega t} \ , \tag{4}$$

where j, m and n denote the index number referring to DoFs of deterministic components, ranging from 1 to N_d; l, p, q are the integer regarding the selected frequency points whose absolute value ranges from 1 to N_l. Similarly for conciseness, the lower limit of the symbol $\sum_{s=1}^{N_d}$ is omitted and it can be simplified to $\sum_s^{N_d}$. The Galerkin method then can be applied to obtain the least weighted residual as

$$\epsilon_{jr}^{H2} = \int_\infty \epsilon_j^{H1} e^{-i\, r\omega t} dt \ . \tag{5}$$

where r is the index ranging from 1 to N_d. It is noted that the above equation can also be seen as the Fourier transform of ϵ_j^{H1}. It is easy to know that the residual ϵ_j^{H1} is a real number, while with the introduction of basis function containing imaginary numbers, the residual ϵ_j^{H2} is a complex number. Substitute Eq.(4) into the Eq.(5), and combine with following relation

$$\int_\infty e^{i\, l\omega t} e^{-i\, r\omega t} dt = 2\pi\delta(l-r) \ , \tag{6}$$

where $\delta()$ is the Kronecker Delta function as follow

$$\delta_{lr} = \begin{cases} 1, & \text{if } l = r, \\ 0, & \text{if } l \neq r. \end{cases} \tag{7}$$

Then the weighted residual can be rewritten as

$$\epsilon_{jr}^{H2} = 2\pi \left[\overline{u}_{jr}(-r^2\omega^2 m_j + ir\omega c_j + k_j^a) + \phi_{jr} - \overline{f}_{jr}^{ex} \right] \ , \tag{8}$$

where ϕ_{jr} is the nonlinear term for jr-th equation such that

$$\phi_{jr} = \sum_{smn}^{N_d} k_{jsmn}^b \sum_{lpq}^{N_\omega} \overline{u}_{sl}\, \overline{u}_{mp}\, \overline{u}_{nq}\, \delta(l+p+q-r) \ . \tag{9}$$

Removing 2π in the Eq.(8) does not affect the derivation. The governing equation in the frequency domain can be rewritten as

$$\epsilon_{jr}^{H2} = \overline{u}_{jr}(-r^2\omega^2 m_j + ir\omega c_j + k_j^a) + \phi_{jr} - \overline{f}_{jr}^{ex} = 0 \ . \tag{10}$$

The number of governing equations of deterministic components is then $2N_\omega \times N_d$. The internal entries in the governing equation are sorted as follow which shows then entries of the response vector $\overline{\mathbf{u}}$ and the residual vector $\boldsymbol{\epsilon}^{H2}$

$$\overline{\mathbf{u}} = \left[\overline{u}_{1(-N_\omega)}, \ldots, \overline{u}_{N_d(-N_\omega)}, \overline{u}_{1(-N_\omega+1)}, \ldots, \overline{u}_{N_d(-N_\omega+1)}, \ldots, \overline{u}_{1N_\omega}, \ldots, \overline{u}_{N_dN_\omega}\right]^T \ , \tag{11}$$

$$\boldsymbol{\epsilon}^{H2} = \left[\epsilon_{1(-N_\omega)}, \ldots, \epsilon_{N_d(-N_\omega)}, \epsilon_{1(-N_\omega+1)}, \ldots, \epsilon_{N_d(-N_\omega+1)}, \ldots, \epsilon_{1N_\omega}, \ldots, \epsilon_{N_dN_\omega}\right]^T \ , \tag{12}$$

where the elements $\overline{\mathbf{u}}_{jr}$ and $\overline{\mathbf{u}}_{j(-r)}$ are conjugate pair, and the real parts of them, as well as the imaginary parts, are fully correlated. The governing equation (10) is a nonlinear algebraic equation. It is difficult to be directly solved when considering the hybrid model. Following the description in the introduction and second section, the linearisation technique is applied here. The equivalent stiffness for the nonlinear terms can be constructed and Eq.(10) becomes

$$\epsilon_{jr}^{H3} = \overline{u}_{jr}(-r^2\omega^2 m_j + ir\omega c_j + k_j^a) + \sum_s^{N_d}\sum_l^{N_\omega} k_{jr,sl}^{eq}\overline{u}_{sl} - \overline{f}_{jr}^{ex} = 0 \ , \tag{13}$$

where $k_{jr,sl}^{eq}$ represents the equivalent stiffness for $\overline{u}_{sl}$ in jr-th equation. Let's define the residual between Eq.(10) and Eq. (13) as

$$\epsilon_{jr}^{eq} = \epsilon_{jr}^{H3} - \epsilon_{jr}^{H2} = \sum_s^{N_d}\sum_l^{N_\omega} k_{jr,sl}^{eq}\overline{u}_{sl} - \phi_{jr} \ . \tag{14}$$

This residual which denotes the difference between nonlinear stiffness and equivalent linear stiffness should be as small as possible, and in this paper the expectation of least square sense of the residual is chosen as the objective function as follow [25]

$$\min_{k^{eq}} \mathbb{E}\left[\|\boldsymbol{\epsilon}^{eq}\|^2\right] \ . \tag{15}$$

where $\mathbb{E}[\cdot]$ denotes the expectation. The equivalent stiffness can be obtained by applying the partial differentiate as

$$\frac{\partial \mathbb{E}[(\boldsymbol{\epsilon}^{eq})^H \boldsymbol{\epsilon}^{eq}]}{\partial k_{jr,vw}^{eq}} = 0 \ , \tag{16}$$

where v is the index regarding the DoFs ($1 \le v \le N_d$); w is the index referring to discretized frequency ($-N_\omega \le w \le -1$ or $1 \le w \le N_\omega$). The equation above can be transformed as

$$\frac{\partial \mathbb{E}\left[\sum_s^{N_d}\sum_l^{N_\omega} \epsilon_{sl}^{eq}(\epsilon_{sl}^{eq})^*\right]}{\partial k_{jr,vw}^{eq}} = \mathbb{E}\left[(\epsilon_{jr}^{eq})^* \frac{\partial \epsilon_{jr}^{eq}}{\partial k_{jr,vw}^{eq}} + \epsilon_{jr}^{eq}\frac{\partial (\epsilon_{jr}^{eq})^*}{\partial k_{jr,vw}^{eq}}\right] = 0 \ . \tag{17}$$

Substituting Eq.(14) into above equation yields

$$\sum_s^{N_d}\sum_l^{N_\omega} k_{jr,sl}^{eq}\,\Re\{\mathbb{E}[\overline{u}_{sl}\overline{u}_{vw}^*]\} = \Re\{\mathbb{E}[\phi_{jr}\overline{u}_{vw}^*]\} \, , \tag{18}$$

where the symbol $\Re\{\cdot\}$ represents the real part of a complex number or a matrix; $\overline{u}$ is the frequency-domain response and is assumed to follow the Gaussian-level distribution.

By implementing Isserlis' theorem (or Wick's probability theorem), the following relation can be obtained

$$\mathbb{E}[u_1 u_2 ... u_n] = \sum_{\pi \in P_2(n)} \prod_{a,b \in \pi} \mathbb{E}[u_a u_b] \tag{19}$$

where $P_2(n)$ denotes the set of all pairs in the set 1,2,...,n. The term $\mathbb{E}[\phi_{jr}\overline{u}^*_{vw}]$ by applying the Isserlis' theorem becomes

$$\mathbb{E}[\phi_{jr}\overline{u}^*_{vw}] = \sum_s \sum_l \mathbb{E}\left[\overline{u}_{sl}\overline{u}^*_{vw}\right] \sum_{m,n}^{N_d} (k^b_{jsmn} + k^b_{jmsn} + k^b_{jmns}) \sum_{p,q}^{N_\omega} \mathbb{E}[\overline{u}_{mp}\overline{u}_{nq}]\, \delta(l+p+q-r)\,. \tag{20}$$

The equation above contains the term $\mathbb{E}\left[\overline{u}_{mp}\overline{u}_{nq}\right]$, but in the hybrid model, the term $\mathbb{E}\left[\overline{u}_{mp}\overline{u}^*_{nq}\right]$ is usually referred. Hence, it is necessary to transform the formula of the front to the later. The conjugate pair of the response in positive and negative frequencies has been used in Eq. (2), and one element of the pair shares the same statistics with the other for both the real and imaginary part. This means $\mathbb{E}\left[\overline{u}_{mp}\overline{u}_{nq}\right] = \mathbb{E}\left[\overline{u}_{mp}\overline{u}^*_{n(-q)}\right]$ can be used. Substitute this equation into Eq. (20) gives

$$\mathbb{E}[\phi_{jr}\overline{u}^*_{vw}] = \sum_s \sum_l \mathbb{E}\left[\overline{u}_{sl}\overline{u}^*_{vw}\right] \sum_{m,n}^{N_d} (k^b_{jsmn} + k^b_{jmsn} + k^b_{jmns}) \sum_{p,q}^{N_\omega} \mathbb{E}[\overline{u}_{mp}\overline{u}^*_{n(-q)}]\, \delta(l+p+q-r)\,. \tag{21}$$

We can rewrite Eq.(18) in the matrix form as

$$\mathbf{K}^{eq}\ \Re\{\mathbf{S}^{uu}\} = \Re\{\mathbf{\Phi}\}\ , \tag{22}$$

where

$$\begin{aligned}
\mathbf{S}^{uu}_{IJ} &= \mathbb{E}[\overline{u}_{jr}\overline{u}^*_{vw}]\,, \\
\mathbf{\Phi}_{IJ} &= \mathbb{E}[\phi_{jr}\overline{u}^*_{vw}]\,, \\
I &= \begin{cases} N_d(r+N_\omega)+j\ , & \text{if } r<0\ , \\ N_d(r-1+N_\omega)+j\ , & \text{if } r>0\ , \end{cases} \\
J &= \begin{cases} N_d(w+N_\omega)+v\ , & \text{if } w<0\ , \\ N_d(w-1+N_\omega)+v\ , & \text{if } w>0\ . \end{cases}
\end{aligned}$$

and I and J are the indices of an entry in the matrix.

In fact, the equivalent stiffness $\mathbf{K}^{eq}$ have centrosymmetric property due to the introduction of positive and negative frequencies. It can be obtained from previous discussion that $\mathbb{E}\left[\overline{u}_{s(-l)}\overline{u}^*_{vw}\right] = \mathbb{E}\left[\overline{u}^*_{sl}\overline{u}_{v(-w)}\right]$. And from Eq. (9), it can be easily shown that ϕ_{jr} and $\phi_{j(-r)}$ are also conjugate pair. This similarly results in $\mathbb{E}[\phi_{j(-r)}\overline{u}^*_{vw}] = \mathbb{E}[\phi^*_{jr}\overline{u}_{v(-w)}]$. These two equations lead to the centrosymmetry property of $\Re\{\mathbf{S}^{uu}\}$ and $\Re\{\mathbf{\Phi}\}$ in terms of the blocks as

$$\begin{aligned}
\Re\{\mathbf{S}^{uu}\}_{jr,vw} &= \Re\{\mathbf{S}^{uu}\}_{j(-r),v(-w)}\ , \\
\Re\{\mathbf{\Phi}\}_{jr,vw} &= \Re\{\mathbf{\Phi}\}_{j(-r),v(-w)}\ .
\end{aligned}$$

Then it can be inferred that the equivalent stiffness matrix meets the same property as

$$\Re\left\{\mathbf{K}^{eq}\right\}_{jr,vw} = \Re\left\{\mathbf{K}^{eq}\right\}_{j(-r),v(-w)} \tag{23}$$

This property is important since it can be used to save the computational resources when calculating the equivalent stiffness matrix.

3.2. Linearised governing equation and hybrid model

Rewriting Eq.(13) in matrix form yields

$$\left(\mathbf{D} + \mathbf{K}^{eq}\right)\overline{\mathbf{u}} = \mathbf{D}_{det}\overline{\mathbf{u}} = \overline{\mathbf{f}}^{ex} \ , \tag{24}$$

where $\mathbf{D}$ is the dynamic stiffness matrix of the deterministic linear component; $\mathbf{K}^{eq}$ is the equivalent stiffness matrix; $\mathbf{D}_{det}$ is the linearised dynamic stiffness matrix for deterministic components. Then the entries of the matrices and vectors in Eq.(24) can be written as

$$\mathbf{K}^{eq}_{IJ} = k^{eq}_{jr,vw} \ , \ \overline{\mathbf{u}}_I = \overline{u}_{jr} \ , \ \overline{\mathbf{f}}^{ex}_I = \overline{f}^{ex}_{jr} \ .$$

The governing equation (24) essentially includes all the responses within the calculating frequency range. Hence, the order of $\mathbf{D}_{II}$ can be tremendous if the number N_ω is large. But the advantage is that with a single calculation, the response within the frequency range of analysis can be obtained.

Denoting the number of subsystems of pure linear built-up system as N_s and currently considering each original subsystem at every selected frequency as one subsystem, the number of total subsystem becomes $N_{tot} = 2N_\omega \times N_s$. In the following derivation, we define

$$M = \begin{cases} N_s(r + N_\omega) + s \ , & \text{if } r < 0 \ , \\ N_s(r - 1 + N_\omega) + s \ , & \text{if } r > 0 \ , \end{cases} \tag{25}$$

$$N = \begin{cases} N_s(l + N_\omega) + t \ , & \text{if } l < 0 \ , \\ N_s(l - 1 + N_\omega) + t \ , & \text{if } l > 0 \ . \end{cases} \tag{26}$$

where r and l represent the indices for the frequency $r\omega$ and $l\omega$, and meet the conditions of $-N_\omega \leq r, l \leq -1$ or $1 \leq r, l \leq N_\omega$; s and t are the indices related to the number of original subsystems N_s, and satisfy these inequities $1 \leq s, t \leq N_s$. Coupling the deterministic governing equation (24) to the statistical fields which are the superposition of direct fields and reverberant fields, the governing equation of the structural system can be written as

$$\mathbf{D}_{tot}\,\overline{\mathbf{u}} = \overline{\mathbf{f}}^{ex} + \sum_{M}^{N_{tot}} \mathbf{f}^{rev}_{(M)} \ , \tag{27}$$

$$\mathbf{D}_{tot} = \mathbf{D} + \mathbf{K}^{eq} + \sum_{M}^{N_{tot}} \mathbf{D}^{dir}_{(M)} \ , \ , \tag{28}$$

where $\mathbf{f}^{rev}_{(M)}$ is the force vector by M-th reverberant field; $\mathbf{D}^{dir}_{(M)}$ is direct field matrix of M-th subsystem. It should be noted that due to the introduction of negative frequencies, the non-zero entries of $\mathbf{D}^{(dir)}_{(M)}$ should

have a pair which refer to frequency pairs, and the pairs are conjugate. From Eq.(27), the equation regarding the cross-spectral matrix of the deterministic components can be obtained as

$$\mathbf{S}^{uu} = (\mathbf{D}_{tot})^{-1} \left(\mathbf{S}^{ff} + \sum_{M}^{N_{tot}} \mathbf{S}^{rev}_{(M)} \right) (\mathbf{D}_{tot})^{-H} , \tag{29}$$

where

$$\mathbf{S}^{ff}_{IJ} = \mathbb{E}\left[\bar{\mathbf{f}}^{ex}_{I} (\bar{\mathbf{f}}^{ex}_{J})^{H} \right] , \quad \mathbf{S}^{rev}_{(M)} = \mathbb{E}\left[\mathbf{f}^{rev}_{(M)} (\mathbf{f}^{rev}_{(M)})^{H} \right] . \tag{30}$$

According to the reciprocity relation, the cross-spectral matrix of force by reverberant field can be written as [9]

$$\mathbf{S}^{rev}_{(M)} = \frac{4E_M}{\pi r \omega n_s} \mathrm{Im}\left\{ \mathbf{D}^{dir}_{(M)} \right\} . \tag{31}$$

Considering the ensemble and time average power flow in reverberant fields of the subsystems, the power balance requires that the power into a subsystem should equal the sum of the power dissipated within the subsystem and the power flowing out to others. The power balance in the j-th subsystem can then be written as

$$P^{in}_{M} = P^{rev}_{out,M} + P^{diss}_{M} , \tag{32}$$

where P^{in}_{M} is the power injected into the M-th subsystem; $P^{rev}_{out,M}$ is the power flowing out of M-th reverberant field; P^{diss}_{M} is the power dissipated in M-th subsystem. P^{in}_{M} is given as

$$P^{in}_{M} = \frac{1}{2} \sum_{mn} \mathrm{Im}\left[\mathbf{w} \mathbf{D}^{dir}_{(M)} \right]_{mn} [\mathbf{S}^{uu}]_{mn} , \tag{33}$$

where

$$\mathbf{w} = \begin{bmatrix} \mathbf{w}_{-N_\omega} & & & & \\ & \ddots & & & \\ & & \mathbf{w}_r & & \\ & & & \ddots & \\ & & & & \mathbf{w}_{N_\omega} \end{bmatrix} , \mathbf{w}_r = \begin{bmatrix} r\omega & & \\ & \ddots & \\ & & r\omega \end{bmatrix}_{N_d \times N_d} . \tag{34}$$

Combining Eq.(29), (31) and (33), the input power can be rewritten as

$$P^{in}_{M} = P^{ext}_{M} + \sum_{N}^{N_{tot}} n_s \eta_{MN} \frac{E_N}{n_t} , \tag{35}$$

where

$$P^{ext}_{M} = \frac{1}{2} \sum_{mn} \mathrm{Im}\left[\mathbf{w} \mathbf{D}^{dir}_{(M)} \right]_{mn} \left[\mathbf{D}^{-1}_{tot} \mathbf{S}^{ff} \mathbf{D}^{-H}_{tot} \right]_{mn} , \tag{36}$$

$$n_s \eta_{MN} = \frac{2}{\pi l \omega} \sum_{mn} \mathrm{Im}\left[\mathbf{w} \mathbf{D}^{dir}_{(M)} \right]_{mn} \left[\mathbf{D}^{-1}_{tot} \mathbf{D}^{dir}_{(N)} \mathbf{D}^{-H}_{tot} \right]_{mn} . \tag{37}$$

The power flowing out of the reverberant field from M-th subsystem can be written as

$$P^{rev}_{out,M} = \frac{1}{2} \sum_{mn} \mathrm{Im}\left[\mathbf{w} \mathbf{D}_{tot} \right]_{mn} \left[\mathbf{S}^{rev}_{qq,(M)} \right]_{mn} . \tag{38}$$

Substituting Eq.(29) and (31) into above equation gives

$$P_{out,M}^{rev} = \sum_{N} n_t \eta_{NM} \frac{E_M}{n_s} + \eta_{d,M} E_M \ , \tag{39}$$

where

$$\eta_{d,M} = \frac{2}{\pi r \omega n_s} \sum_{mn} \mathrm{Im}\left[\mathbf{w}\mathbf{D}_{det}\right]_{mn} \left[\mathbf{D}_{tot}^{-1}\mathbf{D}_{(M)}^{dir}\mathbf{D}_{tot}^{-H}\right]_{mn} \ , \tag{40}$$

is related to the power dissipated in deterministic components. Then the power dissipated within the M-th subsystem P_M^{diss} reads

$$P_M^{diss} = |r|\omega \, \eta_M \, E_M \ , \tag{41}$$

where η_M is the damping loss factor.

Substituting Eq.(35), (39) and (41) into power balance equation (32) gives

$$\left(|r|\omega\eta_M + \eta_{d,M}\right) E_M + \sum_{N}^{N_{tot}} \eta_{MN} \, n_s \left(\frac{E_M}{n_s} - \frac{E_N}{n_t}\right) = P_{ext,M} + P_M^{in,M} \ . \tag{42}$$

Substitute the reciprocity equation (31) into Eq.(29), then the response cross-spectral matrix of deterministic component can be written as

$$\mathbf{S}^{uu} = \mathbf{D}_{tot}^{-1}\left[\mathbf{S}^{ff} + \sum_{M}^{N_{tot}} \left(\frac{4E_M}{\pi r \omega n_s}\right) \mathrm{Im}\left\{\mathbf{D}_{(M)}^{dir}\right\}\right] \mathbf{D}_{tot}^{-H} \ . \tag{43}$$

The procedure obtaining the ensemble average energy for subsystems and cross-spectral matrix for deterministic components can be summarised as follows

1. Ignore the nonlinear terms of the governing equation and calculate the linear response.
2. Obtain equivalent stiffness matrix $\mathbf{K}^{eq}$ by Eq.(22).
3. Substitute $\mathbf{K}^{eq}$ into the governing equation (24), and obtain the cross-spectral matrix of the deterministic components and the ensemble average energy of the subsystems.
4. Calculate the $\mathbf{K}^{eq}$ and its error. Substitute current $\mathbf{K}^{eq}$ into the third step if the error is larger than the tolerance. Or terminate the iterations if the error is smaller than the tolerance.

4. Benchmark model

This section introduces a benchmark model for validation purpose. This model is similar to the one used in previous investigations [21]. The difference is that the deterministic components in this paper are sets of nonlinear spring-mass systems. This model can be extended to more complex deterministic components, which is demonstrated in following case study. In the current model, the two isotropic, homogeneous and linear elastic rectangular plates coupled by nonlinear springs-mass structures are taken into account. The geometry and schematic representations are shown in Fig.4. In this system, the plates are simply supported and the upper plate is subjected to a concentrated harmonic force with a constant direction of vertical downward. Each plate of the whole dynamic system is randomized by using lumped masses which are randomly distributed on the plates. The LRRM based on the weak-form of governing equations of the bare

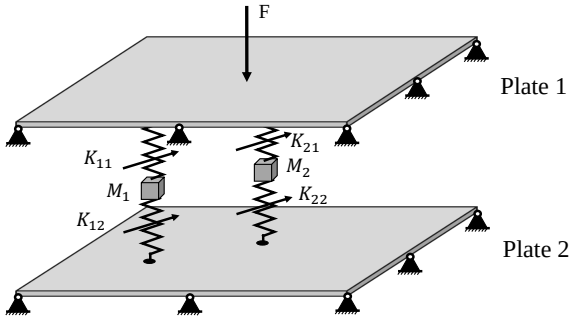

Figure 4: Schematic figure for case 1

plate is employed as solving method [21]. In this context, the transverse displacement $w(x, y, t)$ can be expanded into a Ritz sense as follows

$$w(x, y, t) = \sum_{mn} \psi_{mn}(\mathbf{x}) q_{mn}(t) \ , \tag{44}$$

where the modal coordinates q_{mn} are time-dependent functions; ψ_{mn} are mass-normalized shape functions. By applying the LRRM (the derivation can be referred to Ref. [21]), the governing equations can be obtained as

$$\begin{aligned} &\ddot{q}_{1,mn} + \omega_{1,mn}^2 q_{1,mn} + \sum_{k=1}^{N_{1,m}} m_k \sum_{ij} \ddot{q}_{1,ij} \psi_{1,ij}(\mathbf{x}_{m_k}) \psi_{1,mn}(\mathbf{x}_{m_k}) \\ &+ \sum_{j}^{N_{sm}} k_{1,j}^1 \left[\sum_{ij} q_{1,ij} \psi_{1,ij}(\mathbf{x}_j) - q_j \right] \psi_{1,mn}(\mathbf{x}_j) \\ &+ \sum_{j}^{N_{sm}} k_{1,j}^3 \left[\sum_{ij} q_{1,ij} \psi_{1,ij}(\mathbf{x}_j) - q_j \right]^3 \psi_{1,mn}(\mathbf{x}_j) \\ &= \overline{F}_1 \sin(\omega t + \phi) \psi_{1,mn} \end{aligned} \tag{45}$$

$$\begin{aligned} &\ddot{q}_{2,mn} + \omega_{2,mn}^2 q_{2,mn} + \sum_{k=1}^{N_{2,m}} m_k \sum_{ij} \ddot{q}_{2,ij} \psi_{2,ij}(\mathbf{x}_{m_k}) \psi_{2,mn}(\mathbf{x}_{m_k}) \\ &+ \sum_{j}^{N_{sm}} k_{2,j}^1 \left[\sum_{ij} q_{2,ij} \psi_{2,ij}(\mathbf{x}_j) - q_j \right] \psi_{2,mn}(\mathbf{x}_j) \\ &+ \sum_{j}^{N_{sm}} k_{2,j}^3 \left[\sum_{ij} q_{2,ij} \psi_{2,ij}(\mathbf{x}_j) - q_j \right]^3 \psi_{2,mn}(\mathbf{x}_j) = 0 \end{aligned} \tag{46}$$

$$\begin{aligned} &M_j \ddot{q}_j + k_{1,j}^1 \left[q_j - \sum_{mn} \psi_{1,mn}(\mathbf{x}_{k_j}) q_{1,mn} \right] + k_{2,j}^1 \left[q_j - \sum_{mn} \psi_{2,mn}(\mathbf{x}_{k_j}) q_{2,mn} \right] \\ &+ k_{1,j}^3 \left[q_j - \sum_{mn} \psi_{1,mn}(\mathbf{x}_{k_j}) q_{1,mn} \right]^3 + k_{2,j}^3 \left[q_j - \sum_{mn} \psi_{2,mn}(\mathbf{x}_{k_j}) q_{2,mn} \right]^3 = 0 \end{aligned} \tag{47}$$

where $N_{1,m}$ and $N_{2,m}$ represent the numbers of random masses on the plates 1 and plate 2, respectively; N_{sm} is the set number of the spring-mass system; m_k is the magnitude of the k-th mass; $\mathbf{x}_{m_k} = (x_{m_k}, y_{m_k})$ is the

randomised coordinate of the mass m_k; where ω_{mn} is the natural frequency of the bare plate; D is the flexural rigidity; $k^1_{1,j}$ and $k^3_{1,j}$ correspond to the linear term and the cubic term of first spring stiffness coefficient in j-th spring-mass system; $k^1_{2,j}$ and $k^3_{2,j}$ correspond to the linear term and the cubic term of second spring stiffness coefficient in j-th spring-mass system; $\mathbf{x}_{k_j} = (x_{k_j}, y_{k_j})$ is the coordinates of the coupling point; where $\overline{F}_1 \sin(\omega t + \phi)$ represents the sinusoidal excitation with amplitude $\overline{F}_1$, circular frequency ω and phase angle ϕ; $\mathbf{x}_{F_1}$ denotes the coordinate of the external force.

This paragraph presents how the deterministic components in hybrid FE-SEA model are specified. It can be observed in Fig.4 that the load in mid-frequency range and along vertical direction excites the out-of-plane motion of plate 1. Then the spring-mass system and the motion of plate 2 also follow the vertical motion. The out-of-plane motion fields of the plates which are vulnerable to uncertainties are considered as SEA subsystems. The spring-mass structures in which the translational springs are assumed to have large stiffness are deterministic joints in this model. It is easy to see that each spring-mass system yields 3 DoFs, one of which denotes the translational motion of the mass, and the others refer to motion of connection points to the plates (deterministic boundaries). Hence, for the structure including two spring-mass systems depicted in Fig.4, the number of DoFs of deterministic components is 6. When constructing the dynamic stiffness $\mathbf{D}_{det}$ for deterministic components, the spring-mass systems are blocked, which means the deterministic boundaries are assumed as free. Denote the displacement vector of j-th spring-mass system as $\mathbf{q}_j = [q_{1j}, q_{2j}, q_{3j}]^T$ in which the displacements are referred to, respectively, the deterministic boundary point in plate 1, the mass M_j, and the deterministic boundary point in plate 2. For j-th spring-mass system under the frequency of $l\omega$, the linear part of dynamic stiffness matrix can be obtained by general modelling process for dynamic structures as

$$\mathbf{D}^{lin}_{det} = \begin{bmatrix} k^1_{1,j} & -k^1_{1,j} & 0 \\ -k^1_{1,j} & -M_j l^2\omega^2 + k^1_{1,j} + k^1_{2,j} & -k^1_{2,j} \\ 0 & -k^1_{2,j} & k^1_{2,j} \end{bmatrix}. \tag{48}$$

The vector denoting nonlinear terms for j-th spring-mass system can be written as

$$\mathbf{V}^{non}_{det} = \begin{bmatrix} k^3_{1,j}(q_{1,j} - q_{2,j})^3 \\ -k^3_{1,j}(q_{1,j} - q_{2,j})^3 + k^3_{2,j}(q_{2,j} - q_{3,j})^3 \\ -k^3_{2,j}(q_{2,j} - q_{3,j})^3 \end{bmatrix}. \tag{49}$$

To obtain the governing equation by current hybrid model, it is also necessary to give the expression for direct field dynamic matrix. For N-th subsystem $\mathbf{D}^{dir}_{(N)}$ related to plate 1 (the index for plate 1 is 1, setting as $t = 1$), the non-zero block in the matrix can be written as follow

$$[\mathbf{D}^{dir}_N]_{N\times N} = \begin{bmatrix} il\omega Z^{im}_1 & 0 & 0 \\ 0 & 0 & 0 \\ 0 & 0 & 0 \end{bmatrix} \tag{50}$$

where $Z^{im}_1 = 8\sqrt{D_{r1}\rho_1 h_1}$ is the infinite-plate impedance related to plate 1; D_{r1}, ρ_1 and h_1 are plate flexural rigidity, density and thickness of plate 1; l is the frequency index; l, t and N satisfy the relation of Eq. (26). For the direct field dynamic matrix related to plate 2 ($t = 2$). the non-zero block in the matrix can be written

as follow

$$[\mathbf{D}_N^{dir}]_{N\times N} = \begin{bmatrix} 0 & 0 & 0 \\ 0 & 0 & 0 \\ 0 & 0 & il\omega Z_2^{im} \end{bmatrix} \tag{51}$$

where $Z_2^{im} = 8\sqrt{D_{r2}\rho_2 h_2}$ is the infinite-plate impedance related to plate 2; D_{r2}, ρ_2 and h_2 are plate flexural rigidity, density and thickness of plate 2.

5. Numerical results

This section targets the validation of the proposed formulation by implementing two case studies. The first case which refers to the geometry model in Fig. 4 has a relative simple coupling relation between two subsystems (plates). The second case is more complex than the first case. The number of subsystems is increased to three, and the connection between first and second plates is related to two nonlinear spring-mass systems in which the masses are coupled by an nonlinear spring. The geometry model is shown in Fig.8. These two cases respectively including simple and complex coupling relation can not only validate the proposed formulation, but also provide remarkable understanding about energy transfer by nonlinear joints. In these two cases, translational springs and Kirchhoff plates are used to construct the structure. The materials of the plates are assumed to be homogeneous, and isotropic with Poisson's ratio $\nu = 0.3$ and damping loss factor 0.01. The dimensions, mass densities and Young's modulus are referred in Tab.1. Some of the translational springs are nonlinear. The stiffness parameters for both linear and nonlinear cubic terms are in Tab.2. For validation purpose, 100 MCS samples are used to calculate the ensemble average energy for the nonlinear systems. 20 lumped masses each of which has 2% of the mass of the plate are randomly distributed on the plates in order to obtain every energy ensemble. For both case studies, the input loads are set to be vertical to the plates. The amplitude for the harmonic load is 1000N, the excitation frequency is set to be 2400 rad/s.

Table 1: Parameters of plates.

Structure	Dimensions	Mass density	Young's module
Plate 1	1.35m×1.20m×0.005m	2700kg/m^3	70 GPa
Plate 2	1.05m×1.20m×0.008m	2700kg/m^3	70 GPa
Plate 3	1.00m×1.05m×0.005m	2700kg/m^3	70 GPa

The first case resembles the benchmark model in Fig.4. But the number of the mass-spring set (deterministic component) is one. Applying the current nonlinear FE-SEA and benchmark formulations, the ensemble average energy of subsystems and the spectra of the deterministic component can be calculated. Figures 5(a)(b) show both linear and nonlinear results for plate 1 and plate 2, and Figs.5(c)(d) show the linear and nonlinear spectral response of the mass(M_1). The responses (ensemble average energy or cross-spectral response) by linear and nonlinear analysis are nearly the same in the frequency range 0 - 4700 rad/s. But for higher frequency range 4700 - 10000 rad/s, the nonlinearity causes obvious scattering in which the responses

Table 2: Parameters of springs.

Spring	Parameter (linear term)	Parameter (cubic term)
K_{11}	$1 \times 10^5 N/m$	$1 \times 10^9 N/m^3$
K_{12}	$2 \times 10^5 N/m$	$2 \times 10^{10} N/m^3$
K_{21}	$1 \times 10^5 N/m$	$1 \times 10^9 N/m^3$
K_{22}	$2 \times 10^5 N/m$	$1 \times 10^{10} N/m^3$
K_c	0	$5 \times 10^9 N/m^3$
K_3	$2 \times 10^5 N/m$	0
K_4	$2 \times 10^5 N/m$	0

within the frequency range are larger than the responses by pure linear analysis. The responses between the LRRM+MCS and nonlinear FE-SEA analysis have good agreements in most frequency range, except some local peak points. Figure 6(a) shows the CLF in linear case. It is obvious that the coupling between plate 1 and plate 2 only happens at the same frequency, which conforms to the energy transfer model in Fig.2. Figures 6(b)(c)(d) are the nonlinear CLF within the plates or between the plates. A feature can be observed that several ridges exist in the figures. These ridges essentially reflect the energy scattering between frequency ranges, and it is caused by nonlinearity and can be reflected in Eq. (20) (the Kronecker Delta functions in this equation show the relation between certain frequencies). The data is collected from iteration shown in Fig. 7, points of which are selected at two local peaks with frequency equalling 7200 rad/s and 8600 rad/s. It shown that for proposed formulation, it only takes two iterations to converge. And in current case study, the energy scattering prediction is good for the second peak (frequency at 8600 rad/s) since the error for nonlinear results is very small. But the error at the local peak (7200rad/s) is large, around 10 dB.

The second case as shown in Fig.8 has two coupled sets of mass-spring systems connecting plate 1 and plate 2. Additional nonlinear spring connects the mass M_1 and M_2 in vertical direction. All these springs are nonlinear. Plate 2 and plate 3 are coupled by two linear translational springs. Applying the proposed formulation and LRRM+MCS analysis, both linear and nonlinear results can be seen in Fig.9. Good agreements of results between proposed formulation and benchmark model can be observed in most frequency range. There exist large energy response or frequency error in the local peak in higher frequency range. Figures 10(a)(b) are the CLF from nonlinear FE-SEA analysis. Figure 10(a) denotes the coupling between plate 1 and plate 2. It has the same features observed in the first case. But in Fig.10(b) the coupling between plate 2 and plate 3 happens in the same frequency, which means the coupling is nearly linear, and nonlinear connection between plate 1 and plate 2 has little effects on the coupling between plate 2 and plate 3. Figures 11 show the response at selected frequencies of 7200 rad/s and 8600 rad/s. It can be seen that at the peaks caused by energy scattering, relative large errors (around 10 dB) happened in this case study. We can obverse that the responses by proposed formulation agree with those by benchmark models, except the peak by nonlinear analysis at 7200 rad/s. In fact, if we look at the MCS samples in Fig.9, some samples at these peaks have larger energy level(almost equal to those by nonlinear FE-SEA), but some other samples which are immersed by MCS sample clouds are much smaller. Then the average of all the samples causes a "middle peak". We could guess that at the peak point, the ensemble systems demonstrate different energy scattering features,

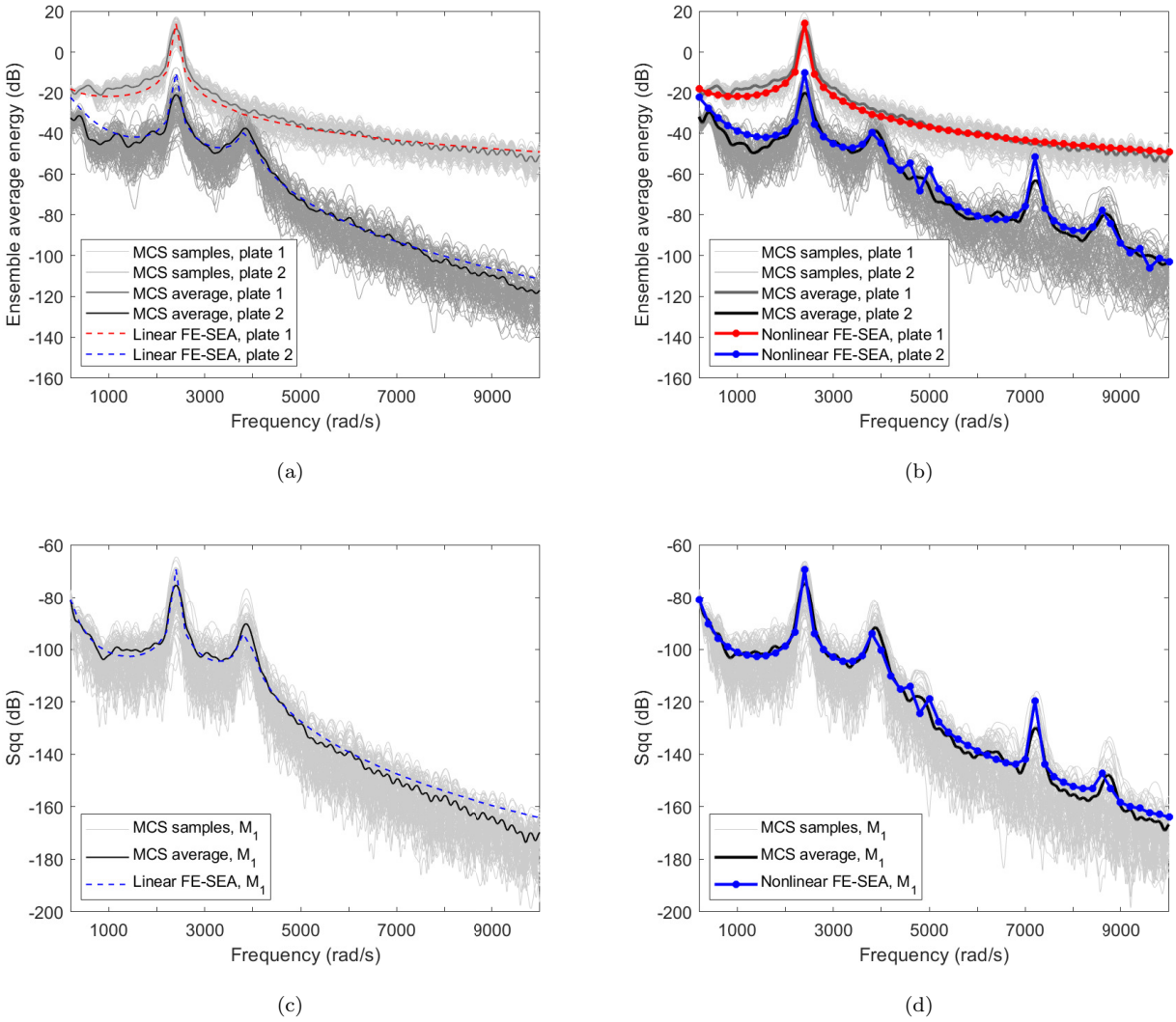

Figure 5: Ensemble average response for the plates and the mass M_1; (a)(b) linear and nonlinear average energy for plates; (c)(d) linear and nonlinear spectral response for the deterministic component M_1.

.

and our proposed formulation catches some but not all of them.

This paragraph discusses the performance of the proposed formulation. In the calculating process [1], only two iterations are needed for both two case studies to converge to the final results. This good convergent performance is due to two reasons. The first one is that the weak nonlinearity assumption keeps most linear features of the models. One obvious feature which can be seen in the figures 5 and 9 is that the linear and nonlinear energy responses in lower frequency range are very close. The second one is that only when it comes to higher frequency range, the energy scattering by nonlinearity significantly affects the energy level. This means not all the frequency calculation point need complex iteration and calculation. The algorithm based on proposed formulation naturally focuses on the higher frequency range but not all the calculating

[1] Computer specifications: processor(Intel(R) Core(TM) i5-8300H CPU); RAM(8.00 GB); system(64-bit Windows 11 system); software (MATLAB R2020b)

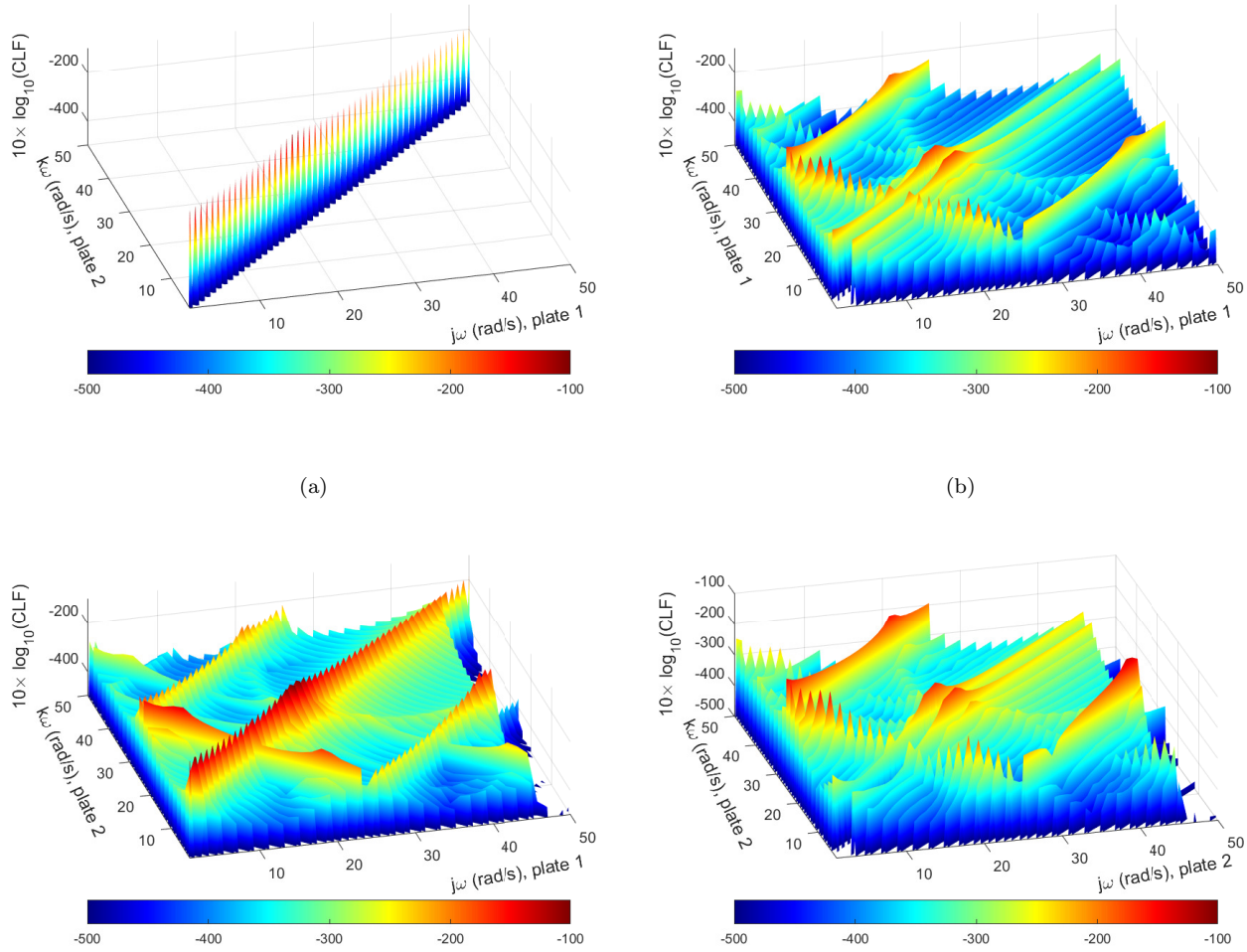

(a) (b)

(c) (d)

Figure 6: (a)CLF between plate 1 and plate 2 by linear analysis; (b) CLF between subsystems within plate 1 by nonlinear analysis; (c) CLF between plate 1 and plate 2 by nonlinear analysis; (d) CLF between subsystems within plate 2 by nonlinear analysis.

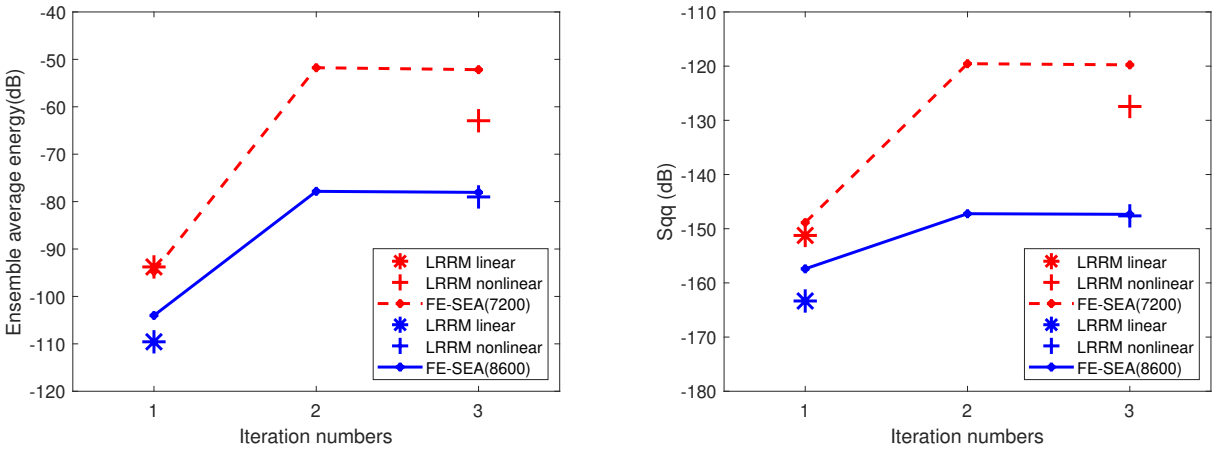

(a) (b)

Figure 7: (a) Linear and nonlinear comparison for energy response of plate 2 at selected frequency equalling 7200 rad/s and 8600 rad/s; (d) Linear and nonlinear comparison for cross-spectral response of the mass M_1 at selected frequency equalling 7200 rad/s and 8600 rad/s.

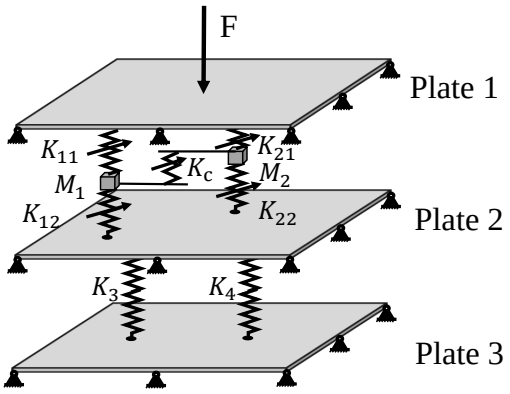

Figure 8: Schematic figure for case 2.

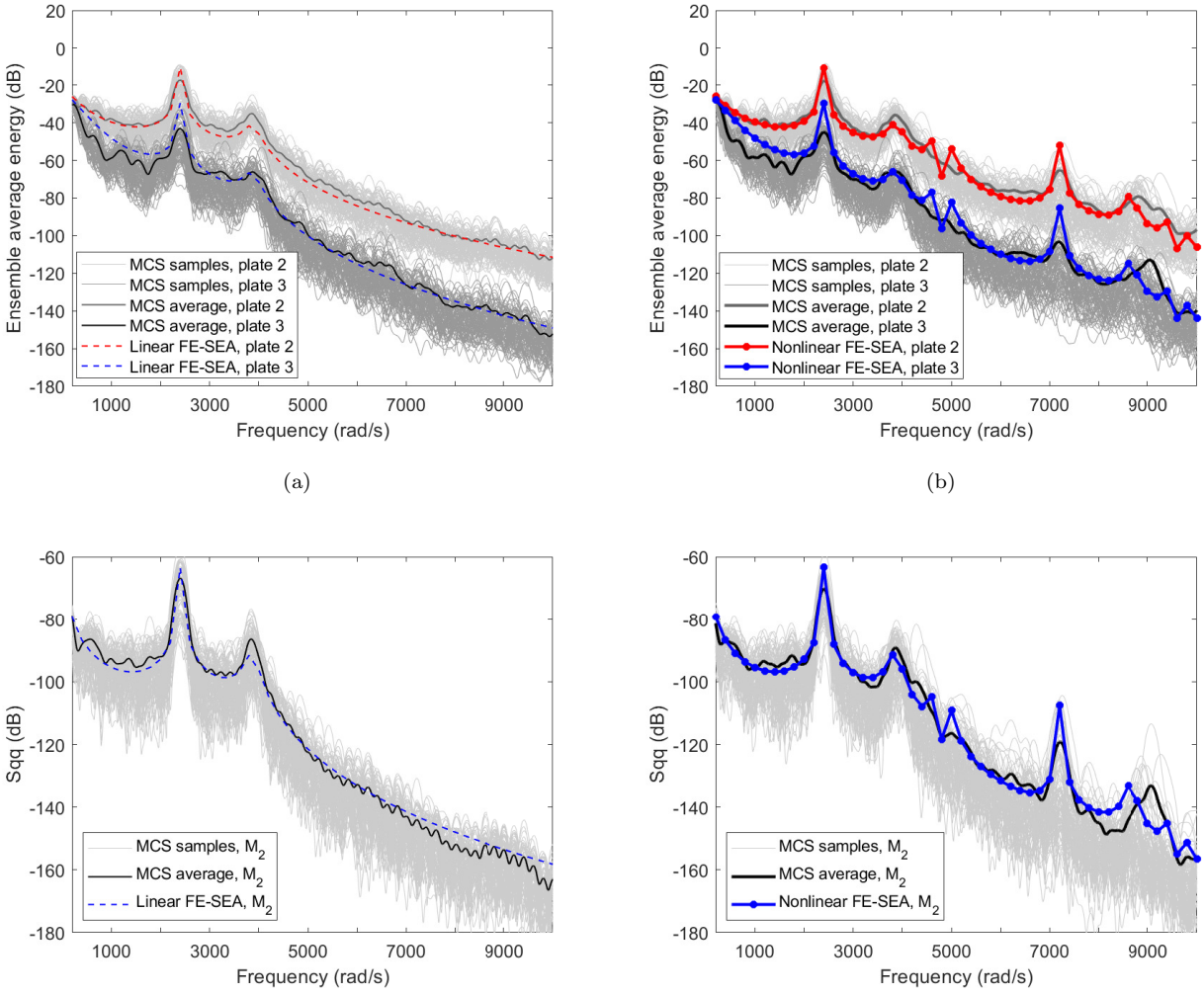

Figure 9: Ensemble average response for the plate 2, 3 and the mass M_2; (a)(b) linear and nonlinear average energy for the plates; (c)(d) linear and nonlinear spectral response for the deterministic component M_2.

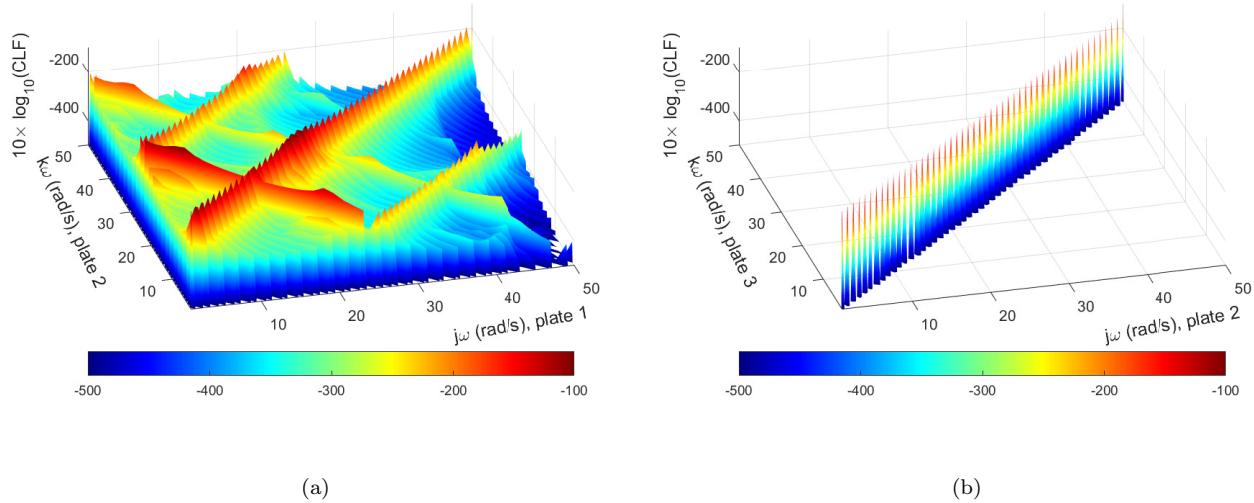

Figure 10: (a)CLF between plate 1 and plate2; (a)CLF between plate 2 and plate 3.

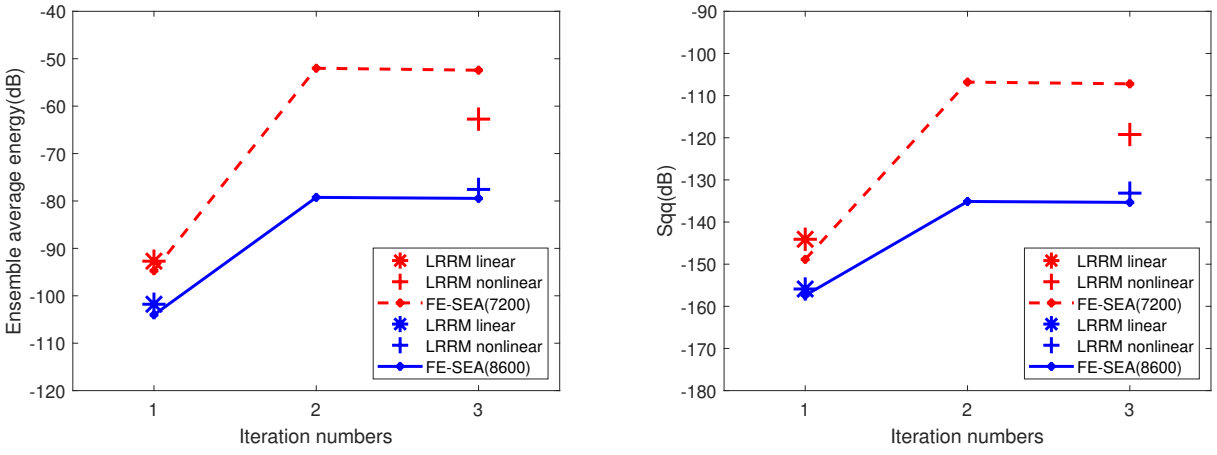

(a) (b)

Figure 11: (a) Linear and nonlinear comparison for energy response of plate 2 at selected frequency equalling 7200 rad/s and 8600 rad/s; (d) Linear and nonlinear comparison for cross-spectral response of the mass M_2 at selected frequency equalling 7200 rad/s and 8600 rad/s.

frequency range. Table 3 shows the computational time for both case studies. It can be observed that when the number of calculating frequency points (N_ω) is small, this algorithm demonstrates very fast performance compared to those obtained by LRRM-MCS. But if the number of frequency points increases, the consumed time increases very significantly. This is because the updating step by Eq. (22) contains too many nested loops, and every layer of loops is related to calculating frequency points N_ω. This means linearly increasing N_ω brings the exponential growth of computational resources. It has been tested in the cases that 40 or 50 frequency points can be the compromise to keep the algorithm efficient and effective enough.

Table 3: Computational cost for case studies; "Nonlinear FE-SEA (30)" refers to $N_\omega = 30$; "Nonlinear FE-SEA (50)" refers to $N_\omega = 50$; LRRM(100) uses 100 MCS samples.

Time(s)	Nonlinear FE-SEA (30)	Nonlinear FE-SEA (50)	LRRM(100)
Case 1	55	324	4386
Case 2	152	2562	8953

6. Conclusion

This paper is devoted to a new hybrid FE-SEA formulation for nonlinear joints. The energy scattering is considered, and this leads to more accurate results in nonlinear cases. This paper proposes a new model for energy transfer between SEA subsystems. And based on this model, the linearisation is realized in frequency domain by MHB plus Galerkin method. This linearisation gives the equation of equivalent stiffness targeting the updating for iterative steps. Two case studies have been given for validation and investigation of the CLF. Good agreements between the benchmark model and proposed hybrid model can be observed.

The formulation in the current paper can be further extended to other types of nonlinearity. The forms of the equivalent stiffness with different nonlinear mathematical forms can be derived in further research.

Previous research of nonlinear hybrid model is limited to simple deterministic components with a very few DoFs. The current nonlinear model is applicable to complex system with MDoF deterministic components. It is noted that the current formulation is limited to weak nonlinearity. But the framework in this paper can be extend to cases with relative larger nonlinearity. But before this extension, some other cases should first be considered; (1) the equilibrium points are not close to zeros; (2) several stable/unstable equilibrium points exists; (3) response distribution with existence of strong linearity (non-Gaussian distribution). Future work relating nonlinear FE-SEA model could focus on these cases.

7. Acknowledgements

The authors would like to thank Dr Fiorenzo Fazzolari for his suggestions and supports to the PhD project (hybrid deterministic-SEA model for complex structures).

References

[1] R. H. Lyon. Statistical energy analysis of dynamical systems. *Theory and Applications*, 1975.

[2] R. H. Lyon, R. G. DeJong, and M. Heckl. Theory and application of statistical energy analysis, 1995.

[3] R. S. Langley and A. W. M. Brown. The ensemble statistics of the energy of a random system subjected to harmonic excitation. *Journal of Sound and Vibration*, 275(3-5):823–846, 2004.

[4] R. S. Langley and A. W. M. Brown. The ensemble statistics of the band-averaged energy of a random system. *Journal of Sound and Vibration*, 275(3-5):847–857, 2004.

[5] F. J. Fahy. Statistical energy analysis: a critical overview. *Philosophical Transactions of the Royal Society of London. Series A: Physical and Engineering Sciences*, 346(1681):431–447, 1994.

[6] A. Le Bot. *Foundation of statistical energy analysis in vibroacoustics*. OUP Oxford, 2015.

[7] P. J. Shorter and R. S. Langley. Vibro-acoustic analysis of complex systems. *Journal of Sound and Vibration*, 288(3):669–699, 2005.

[8] V. Cotoni, P. J. Shorter, and R. S. Langley. Numerical and experimental validation of a hybrid finite element-statistical energy analysis method. *The Journal of the Acoustical Society of America*, 122(1):259–270, 2007.

[9] P. J. Shorter and R. S. Langley. On the reciprocity relationship between direct field radiation and diffuse reverberant loading. *The Journal of the Acoustical Society of America*, 117(1):85–95, 2005.

[10] K. Vergote, B. Van Genechten, D. Vandepitte, and W. Desmet. On the analysis of vibro-acoustic systems in the mid-frequency range using a hybrid deterministic-statistical approach. *Computers & structures*, 89(11-12):868–877, 2011.

[11] R. Gao, Y. Zhang, and D. Kennedy. A hybrid boundary element-statistical energy analysis for the mid-frequency vibration of vibro-acoustic systems. *Computers & Structures*, 203:34–42, 2018.

[12] A. Clot, J. W. R. Meggitt, R. S. Langley, A. S. Elliott, and A. T. Moorhouse. Development of a hybrid FE-SEA-experimental model. *Journal of Sound and Vibration*, 452:112–131, 2019.

[13] C. Fang and Y. Zhang. An improved hybrid FE-SEA model using modal analysis for the mid-frequency vibro-acoustic problems. *Mechanical Systems and Signal Processing*, 161:107957, 2021.

[14] R. S. Langley and V. Cotoni. Response variance prediction in the statistical energy analysis of built-up systems. *The Journal of the Acoustical Society of America*, 115(2):706–718, 2004.

[15] R. S. Langley and V. Cotoni. Response variance prediction for uncertain vibro-acoustic systems using a hybrid deterministic-statistical method. *The Journal of the Acoustical Society of America*, 122(6):3445–3463, 2007.

[16] E. P. B. Reynders and R. S. Langley. Cross-frequency and band-averaged response variance prediction in the hybrid deterministic-statistical energy analysis method. *Journal of Sound and Vibration*, 428:119–146, 2018.

[17] R. S. Langley, D. H. Hawes, T. Butlin, and Y. Ishii. Response variance prediction using transient statistical energy analysis. *The Journal of the Acoustical Society of America*, 145(2):1088–1099, 2019.

[18] A. Carcaterra. Thermodynamic temperature in linear and nonlinear hamiltonian systems. *International Journal of Engineering Science*, 80:189–208, 2014.

[19] R. S. Langley. On the statistical mechanics of structural vibration. *Journal of Sound and Vibration*, 466:115034, 2020.

[20] Z. Sotoudeh. Entropy and mixing entropy for weakly nonlinear mechanical vibrating systems. *Entropy*, 21(5):536, 2019.

[21] F. A. Fazzolari and P. Tan. A hybrid finite element-statistical energy analysis approach for the dynamic response of built-up systems with nonlinear joints. *Journal of Sound and Vibration*, 489:115696, 2020.

[22] F. A. Fazzolari and P. Tan. A linearised hybrid FE-SEA method for nonlinear dynamic systems excited by random and harmonic loadings. *Vibration*, 3(3):304–319, 2020.

[23] L. Andrade, R. S. Langley, and T. Butlin. Equivalent linearisation in a hybrid FE-SEA approach for nonlinear vibro-acoustic modelling. *Journal of Sound and Vibration*, 526:116788, 2022.

[24] G. M. Spelman and R. S. Langley. Statistical energy analysis of nonlinear vibrating systems. *Philosophical Transactions of the Royal Society A: Mathematical, Physical and Engineering Sciences*, 373(2051):20140403, 2015.

[25] J. B. Roberts and P. D. Spanos. *Random vibration and statistical linearization*. Courier Corporation, 2003.

[26] M. Krack and J. Gross. *Harmonic balance for nonlinear vibration problems*, volume 1. Springer, 2019.